Melting Dynamics Beneath the Tonga-Kermadec Island Arc Inferred from ^{231}Pa-^{235}U Systematics

Bernard Bourdon,[1]* Simon Turner,[2] Claude Allègre[1]

Measurement of ^{231}Pa-^{235}U disequilibrium in Tonga-Kermadec island arc lavas (north of New Zealand) permits discrimination of the time scales and mechanisms of fluid addition and partial melting. For Tonga lavas, the ($^{231}Pa/^{235}U$) ratios are less than 1 and can be explained by fluid addition from the subducting plate around 60,000 years ago. In contrast, the effects of partial melting overprinted those of fluid addition in the Kermadec lavas resulting in ($^{231}Pa/^{235}U$) ratios greater than 1.

Island arcs form where oceanic lithosphere is dragged downward beneath an overriding plate. Dehydration of the subducted lithosphere is thought to induce mantle melting responsible for the volcanism at island arcs. A knowledge of the material fluxes beneath subduction zones is important for understanding the formation of new continental crust and also of the recycling of crustal materials back into the convective mantle. An essential concept for characterizing these fluxes of subducted material is the chemical fractionation between elements during fluid-addition and partial melting transfer processes. However, most geochemical tracers necessitate assumptions about their abundances in the mantle wedge before melting. In contrast, parent and daughter nuclides of the U-series decay chain can be assumed to be initially in secular equilibrium and thus record the net effects of fractionation produced during the dehydration and partial melting processes and their time scales. Recent studies of disequilibria between ^{238}U and ^{230}Th have provided information on the time scales of fluid transfer beneath arcs (*1*). Because the various elements in the U-series decay chain have different half-lives and chemical properties, maximum information is provided by studies involving more than one parent-daughter pair (*2*). Few such data are available from arc lavas (*3*) despite the debate on the relative importance of decompression-induced versus fluid-induced melting and the time scales involved (*4–6*). We present a detailed within-arc study by presenting combined ^{231}Pa (half-life of ~32,000 years) and ^{230}Th (half-life of ~75,000 years) data from the Tonga-Kermadec arc.

The intra-oceanic Tonga-Kermadec island arc was formed by westward subduction of the Pacific oceanic plate beneath the Australian plate. The volcanoes along the arc typically erupt basaltic andesites and andesites with subordinate volumes of dacites. Active back-arc spreading has formed the Lau Basin and Havre Trough behind the arc and resulted in the mantle wedge beneath the arc being highly depleted in incompatible elements. Tectonically and seismically, the area is one of the most active on Earth with convergence and back-arc spreading rates increasing northward along the arc (*7*), a consequence of which is wedge depletion increasing northward from Kermadec to Tonga (*8*). This arc has been the focus of much interest, because the depleted composition of the mantle wedge renders it sensitive to additions from the subducting plate and the petrogenesis of the erupted lavas has been studied in detail (*9–11*).

We measured ^{231}Pa-^{235}U disequilibria (*12*) in a series of basaltic andesites chosen to be representative of the compositional range in the arc and which had previously been analyzed for ^{230}Th-^{238}U disequilibria (*10*). The ^{231}Pa concentrations vary from 41 to 122 fg/g while ($^{231}Pa/^{235}U$) ranges from 0.79 to 1.69 (Table 1). The data complement and extend the global survey of Pickett and Murrell (*3*) which revealed ($^{231}Pa/^{235}U$) ratios consistently >1, with the exception of one Fonualei sample from Tonga (Fig. 1A). Whereas both arc segments have excess ^{238}U relative to ^{230}Th, which is thought to reflect U addition by fluids from the subducting slab (*1, 10, 13*), the significant aspect of our dataset is that nearly all of the Tonga samples analyzed have ($^{231}Pa/^{235}U$) ratios <1. In contrast, all but one of the Kermadec lavas have ($^{231}Pa/^{235}U$) ratios >1 (1.12 to 1.69), similar to the previous arc data (*3*). This distinction between the Tonga and Kermadec fields in Fig. 1A suggests a change in the processes controlling ^{231}Pa-^{235}U disequilibria between these arc segments.

The Tonga lavas are typified by ^{235}U excesses, whereas the Kermadec lavas generally have ^{231}Pa excesses. Experimental and empirical data suggest that U should be readily transported by fluids from the subducting plate, whereas Th and Pa are not fluid-mobile (*3, 14*). Thus, the correlated excesses of ^{238}U over ^{230}Th and ^{235}U over ^{231}Pa (Fig. 1A) in the Tonga data can be explained by addition of a U-rich fluid from the subducted slab to the mantle source of the lavas

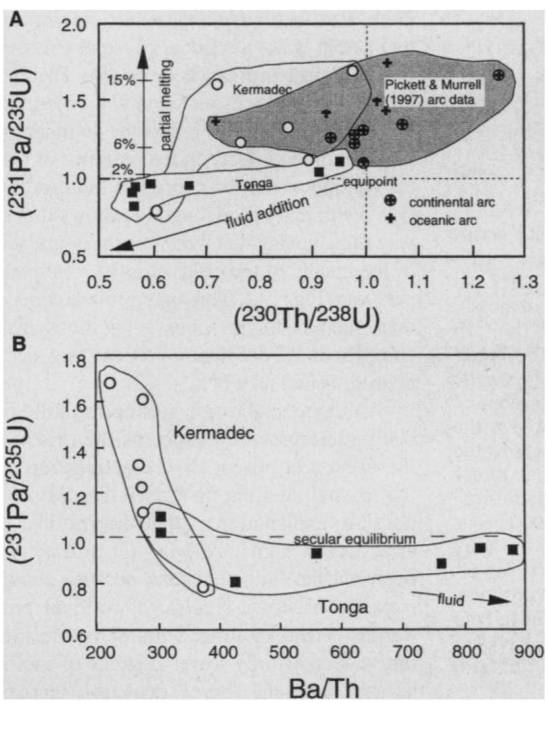

Fig. 1. (**A**) Diagram of ($^{231}Pa/^{235}U$) versus ($^{230}Th/^{238}U$) for the Tonga and Kermadec lavas. The melting trajectory (vertical arrow) is based on calculations of ($^{231}Pa/^{235}U$) using an equilibrium transport model (*18*) with variable clinopyroxene modes in the residue (labels indicate initial percent of clinopyroxene in the residue). Note that with ≤2 to 4% clinopyroxene in the residue, little Pa/U fractionation is produced. (**B**) The correlation between ($^{231}Pa/^{235}U$) and Ba/Th for the Tonga (■) and Kermadec (○) lavas reflects addition of a U-rich slab fluid.

[1]Laboratoire de Géochimie et Cosmochimie, Institut de Physique du Globe de Paris–CNRS, UMR7579, 4 Place Jussieu, 75252 Paris Cedex 05, France. [2]Department of Earth Sciences, The Open University, Milton Keynes MK7 6AA, UK.

*To whom correspondence should be addressed. E-mail: bourdon@ipgp.jussieu.fr

Table 1. The ^{231}Pa-^{235}U disequilibrium data for Tonga-Kermadec lavas.

Sample	U (ppm)	^{231}Pa (fg/g)	(^{231}Pa/^{235}U)†	± (2σ)
		Tonga		
NTT25/4	0.174	57.6	1.026	0.013
NTT29/3	0.168	59.4	1.096	0.010
LATE13	0.206	59.1	0.890	0.014
LATE13 R	0.206	57.4	0.864	0.025
FON31*	0.307	93.3	0.934	0.009
FON39	0.472	122.9	0.807	0.017
26837	0.134	41.3	0.956	0.018
HHTOP	0.133	40.8	0.960	0.030
		Kermadec		
T2	0.164	41.7	0.789	0.033
T5	0.175	63.1	1.117	0.012
4-5653	0.231	120.0	1.611	0.014
37478	0.155	66.4	1.329	0.021
37486	0.191	75.8	1.230	0.014
X162/1	0.215	116.8	1.685	0.028

*Data from (3). †Parentheses denote activity ratios.

(Fig. 1A). This is supported by the observation that Ba/Th ratios, an independent indicator of slab-fluid input (Fig. 1B) (*10*), are also highest in the Tonga rocks.

If we assume that Pa is immobile in fluids like Nb, an "isochron" diagram of (^{231}Pa) versus (^{235}U), both normalized to Nb contents, can be used to assess the time scale of recent fractionation in Pa-Nb relative to U (Fig. 2). The addition of a U-rich fluid should not modify $^{231}Pa/Nb$ ratios, whereas $^{235}U/Nb$ increases. In Fig. 2, all but one of the Tonga lavas fall on a line whose slope yields an age of ~60,000

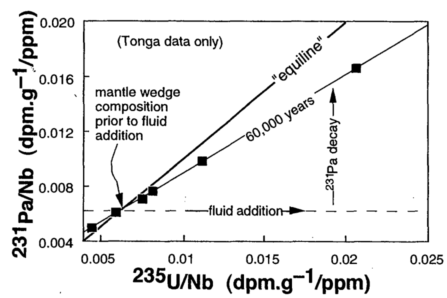

Fig. 2. "Isochron" diagram of ($^{231}Pa/Nb$) versus (^{235}U)/Nb for the Tonga lavas. Units are in decays per minute per gram ($dpm.g^{-1}$) per parts per million. Niobium is used as a chemical analog of Pa; thus, this diagram is similar to the $^{230}Th/^{232}Th$ versus $^{238}U/^{232}Th$ isochron diagram. The "equiline" represents points where ^{231}Pa is in secular equilibrium with its parent ^{235}U and the slope of an isochron line is $1 - e^{-\lambda_{Pa} t}$, where λPa is the decay constant of ^{231}Pa. Samples plotting to the right of the equiline must have undergone recent enrichment in U. The slope of the data array yields an age since U enrichment of 60,000 years. One sample (26837) plotting outside of the array and out of the scale was not used for the regression. The intersection with the equiline constrains the Nb/U ratio in the mantle wedge prior to fluid release and indicates that decrease in Nb/U at subduction zones reflects a combination of both sediment and slab-fluid input.

years. This is in good agreement with the 30,000- to 50,000-year estimate based on ^{230}Th-^{238}U data (*10*). There has been some concern about the validity of interpreting the inclined arrays on ^{238}U-^{230}Th isochron diagrams to record the time since fluid addition beneath arcs, because such arrays could, in theory, reflect mixing with a fluid that contained some Th or mixing between a fluid and variable mantle wedge compositions (*15*). However, the consistency of the Pa-U and U-Th time scales from Tonga provides evidence that such arrays do indeed have age significance with respect to the time since fluid addition. These systematics were not disturbed following fluid addition to the mantle wedge, suggesting that, beneath Tonga, partial melting did not result in significant fractionation of either Th/U or Pa/U (*16*).

An additional process has affected ($^{231}Pa/^{235}U$) in the Kermadec rocks, and since the elevated Ba/Th ratios in these rocks are also consistent with fluid addition to their source (Fig. 1B), the increase in ($^{231}Pa/^{235}U$) is inferred to have occurred during partial melting (*3*). Basalts from mid-ocean ridges and ocean islands are also typified by ^{231}Pa excesses, although these tend to be positively correlated with ^{230}Th excesses, and such Pa-U and Th-U disequilibria are thought to be produced in the presence of residual clinopyroxene ± garnet during partial melting and magma ascent (*2, 3*). Similarly, in the Kermadec data, the largest ^{231}Pa excesses occur in those lavas characterized by the lowest ^{238}U excesses and the data array does not trend toward the equipoint, defined as ($^{231}Pa/^{235}U$) = ($^{230}Th/^{238}U$) = 1 (Fig. 1A). Rather, it is displaced to elevated ($^{231}Pa/^{235}U$) at ($^{230}Th/^{238}U$) = 1, indicating that ^{231}Pa is significantly more incompatible than ^{230}Th (*17*). Rare-earth element modeling indicates that garnet is not a residual phase in the source of the Tonga-Kermadec lavas (*9*). Therefore, the large ^{231}Pa excesses found in the Kermadec lavas are interpreted to reflect the dominance of partial melting effects, in the presence of residual clinopyroxene, over those of fluid addition. Our preliminary modeling (*18*) shows that one way of achieving that would be local upwelling of the mantle of the order of a few centimeters per year (Fig. 1A). This may provide independent support for previous suggestions that a component of decompression melting occurs beneath island arcs (*4*).

An obvious question arising from the preceding interpretation concerns the reason for the limited or absent Pa-U fractionation during partial melting in the Tonga lavas. A possible explanation is that the residual clinopyroxene signature was not sufficient to overprint the fluid signature, because clinopyroxene was not a significant residual phase during partial melting. Clinopyroxene melts out at increasingly lower degrees of melting as the extent of source depletion increases (*19*). Model calculations (*18*) suggest limited Pa-U fractionation during equilibrium transport melting with low clinopyroxene modes (2 to 4%). Thus, melting under these conditions should not greatly affect the Tonga U-Pa systematics and maintain the age consistency with that estimated from U-Th disequilibrium (Fig. 2) (*10*). Further support for this may come from experimental determinations of Pa fluid and melt partitioning.

References and Notes

1. A recent summary is given by C. J. Hawkesworth, S. P. Turner, F. McDermott, D. W. Peate, and P. van Calsteren [*Science* **276**, 551 (1997)].
2. For example, C. C. Lundstrom, J. Gill, Q. Williams, B. B. Hanan, *Earth Planet. Sci. Lett.* **157**, 167 (1998); B. Bourdon, J.-L. Joron, C. Claude-Ivanaj, C. J. Allègre, *Earth Planet. Sci. Lett.* **164**, 119 (1998).
3. D. A. Pickett and M. T. Murrell, *Earth Planet. Sci. Lett.* **148**, 259 (1997).
4. T. Plank and C. H. Langmuir, *Earth Planet. Sci. Lett.* **90**, 349 (1988); J. A. Pearce and I. J. Parkinson, *Geol. Soc. Spec. Publ.* **76**, 373 (1993).
5. J. H. Davies and D. J. Stevenson, *J. Geophys. Res.* **97**, 2037 (1992).
6. D. M. Miller, S. L. Goldstein, C. H. Langmuir, *Nature* **368**, 514 (1994); E. Stolper and S. Newman, *Earth Planet. Sci. Lett.* **121**, 293 (1994).
7. M. Bevis *et al.*, *Nature* **374**, 249 (1995).
8. Indices of depletion, such as low Al/Ti and Ca/Ti ratios and Na and Fe contents, increase northward from Kermadec to Tonga concomitant with increases in the complexity and rate of back-arc spreading (*9, 10*).
9. A. Ewart and C. J. Hawkesworth, *J. Petrol.* **28**, 495 (1987); A. Ewart, K. D. Collerson, M. Regelous, J. I. Wendt, Y. Niu, *J. Petrol.* **39**, 331 (1998).
10. S. Turner and C. Hawkesworth, *Nature* **389**, 568 (1997); S. Turner *et al.*, *Geochim. Cosmochim. Acta* **61**, 4855 (1997).
11. M. Regelous, K. D. Collerson, A. Ewart, J. I. Wendt, *Earth Planet. Sci. Lett.* **150**, 291 (1997).
12. Protactinium-231 concentrations were measured following the technique described by B. Bourdon, J.-L. Joron, and C. J. Allègre [*Chem. Geol.* **157**, 147 (1999)].
13. C. J. Allègre and M. Condomines, *Nature* **299**, 21 (1982).
14. J. M. Brenan, H. F. Shaw, F. J. Ryerson, D. L. Phinney, *Geochim. Cosmochim. Acta* **59**, 3331 (1995); H. Keppler *Nature* **380**, 237 (1996). Protactinium has been shown to be a very insoluble element in aqueous solutions [R. Guillaumont, G. Bouissières, R. Muxart, *Actinides Rev.* **1**, 135 (1968)].
15. T. Elliott, T. Plank, A. Zindler, W. White, B. Bourdon, *J. Geophys. Res.* **102**, 14991 (1997).
16. The melting process has to have reproducibly fractionated Pa/U by the same amount to preserve the isochron relationship in Fig. 2. If we assume 50,000 years elapsed since U addition, based on U-Th data (*9*), the Pa enrichment relative to U due to melting cannot have been greater than ~10%.
17. It has been argued that Pa should be more incompatible than U in clinopyroxene on the basis of the behavior of U^{5+}, a chemical analog of Pa^{5+} [C. C. Lundstrom *et al.*, *Earth Planet. Sci. Lett.* **128**, 407 (1994)]. Theoretical calculations based on the model of Blundy and Wood (*18*) yield D^{Pa} in clinopyroxene = 10^{-5} (B. Wood and J. Blundy, personal communication).
18. The partial melting vector in Fig. 1A was calculated using the model from M. Spiegelman and T. Elliott [*Earth Planet. Sci. Lett.* **118**, 1 (1993)], with the following parameters: *D* values from (*2*) and bulk *D* decreases with degree of melting as in (*2*), porosity ϕ = 1 per mil, degree of melting *F* = 10%, and upwelling rate = 3 cm/year. Source is in secular equilibrium prior to melting. An alternative model is the interaction of melts with the mantle wedge as in B. Bourdon *et al.* (*2*) (AFC-type model). However, for a depleted mantle wedge, this requires unreasonably

large degrees of interaction (>50% crystallization of olivine). Model parameters: $U_{wedge} = 3$ ppb, $U_{melt} = 0.2$ ppm, $r = 0.1$, $D_{wedge} = 6 \times 10^{-3}$.
19. In fertile peridotite, clinopyroxene remains a residual phase until ~22% melting [A. L. Jaques and D. H. Green, *Contrib. Mineral. Petrol.* **73**, 287 (1980)]. However, peridotites depleted by ~7% melt extraction, such as the Tinaquillo spinel iherzolite, contain less clinopyroxene; consequently, this ceases to be a residual phase after only ~8% partial melting [J. A. C. Robinson and B. J. Wood, *Earth Planet. Sci. Lett.* **164**, 277 (1998); L. E. Wasylenski, M. B. Baker, M. M. Hirschmann, E. M. Stolper, *Eos (Fall Suppl.)* **77**, F847 (1996)].
20. We are grateful to A. Ewart, T. Worthington, S. Acland, J. Pearce, A. Reay, I. Smith, and J. Gamble for their generosity in providing samples and to J. L. Joron for his help. We also thank C. Hawkesworth for helpful discussions and careful reading of the manuscript. Careful reviews by R. Arculus and anonymous reviewers led to significant improvements. B.B. was funded by CNRS and S.T. by a Royal Society Research Fellowship. This is IPGP contribution no. 1647.

24 August 1999; accepted 2 November 1999

Gas-Rich Galaxy Pair Unveiled in the Lensed Quasar 0957+561

P. Planesas,[1]* J. Martín-Pintado,[1] R. Neri,[2] L. Colina[3]

Molecular gas in the host galaxy of the lensed quasar 0957+561 (QSO 0957+561) at the redshift of 1.41 has been detected in the carbon monoxide (CO) line. This detection shows the extended nature of the molecular gas distribution in the host galaxy and the pronounced lensing effects due to the differentially magnified CO luminosity at different velocities. The estimated mass of molecular gas is about 4×10^9 solar masses, a molecular gas mass typical of a spiral galaxy like the Milky Way. A second, weaker component of CO is interpreted as arising from a close companion galaxy that is rich in molecular gas and has remained undetected so far. Its estimated molecular gas mass is 1.4×10^9 solar masses, and its velocity relative to the main galaxy is 660 kilometers per second. The ability to probe the molecular gas distribution and kinematics of galaxies associated with high-redshift lensed quasars can be used to improve the determination of the Hubble constant H_0.

Little is known about the contents of molecular gas in galaxies or quasi-stellar objects (quasars) at high redshift, and even less is known about the molecular gas distribution and kinematics. Such knowledge is essential to understanding the evolution of galaxies that are experiencing phases of high activity, in the form of active galactic nuclei or a massive starburst. The relation of the quasar phenomenon to galaxy interaction or merger (*1*) and to star formation activity (*2*) and its possible evolutionary link with luminous infrared galaxies (*3*) are the subjects of a debate that could be better framed if molecular gas distribution and kinematics at high redshift were available. Indeed, the molecular gas presumably constitutes the reservoir that feeds the quasar and the star formation activity (*4*).

Gravitational lenses have recently become a powerful tool for probing the molecular gas content in galaxies at high redshift ($z > 1$). At present, CO emission, the best tracer of molecular gas mass, has been detected in nine objects at redshifts between 2.3 and 4.7 (*5*). Magnification of the emitted spectral lines by a gravitational lens has helped to make the CO emission detectable in at least five cases (*5*). All of these objects, except the quasar APM 08279+5255 (*6*), appear to be one order of magnitude richer in molecular gas than the Milky Way, making them prime candidates for huge starbursts that could not be maintained for a long period of time. It has been suggested that the exhaustion of the molecular gas could lead to the end of the quasar activity (*7*) and eventually to the evolution of the host galaxy, an interacting spiral, toward an elliptical galaxy (*8*).

Between 6 May and 25 December of 1998, we observed the 3.1-mm radio continuum and the CO 2 → 1 (*9*) emission of the twin QSO 0957+561, the first example of gravitational lensing, unambiguously identified 20 years ago (*10*). We used the radio interferometer of the Institute de Radio Astronomie Millimétrique (IRAM) located at Plateau de Bure (France). Three interferometer configurations of the five 15-m-diameter antennas were used, giving 27 hours of useful data on the source and an angular resolution of 3.2″ by 3.1″. The radio continuum (Fig. 1) and the spectral line of CO (Fig. 2) were detected. The line appears redshifted to 95.5 GHz for $z = 1.4141$. Simultaneous observation at the redshifted frequency of the CO 5 → 4 line (238.7 GHz) gave no detection of such a line or of the radio continuum because of insufficient sensitivity at this higher observing frequency. The 3σ limit for the line detection was 5.5 mJy per beam [1 jansky (Jy) = 10^{-26} W m^{-2} Hz^{-1}] for a velocity resolution of 50 km s^{-1}.

The radio continuum map at a wavelength of 3.1 mm (Fig. 1) shows three components that, within the measurement uncertainties, agree in position with optical images A and B (*11*), whereas source C is the northeastern lobe of the radio jet associated with A (*12*). The integrated fluxes for sources A, B, and C are 4.4, 2.6, and 7.2 mJy, respectively. The B/A flux ratio is 0.6, similar to the ratio obtained at lower frequencies with the Very Large Array (VLA) radio interferometer (*13*) and in the near infrared (*14*). The 20-mm to 3-mm spectral index for quasar images A and B is $\alpha = -0.6$ ($S \propto \nu^{\alpha}$), which is somewhat less steep than that at longer wavelengths (S is the flux at a frequence ν).

The picture that emerges from the CO 2 → 1 line observations (Table 1 and Fig. 2) is much more complex than that of the radio continuum and optical images (*11*). Two images, CO-A and CO-B, lay close to the radio and optical A and B images (Table 1), separated from them by ~0.4″. The CO-B image is a highly distorted arc, extended in the east-west direction. A third image of the molecular gas emission, CO-F, with no counterpart in the radio continuum or optical wavelengths, is connected to the CO-B image by a weak arclike structure. The resulting overall picture is interpreted as being produced by the lens acting on an extended distribution of the molecular gas in the host galaxy. Arcs are

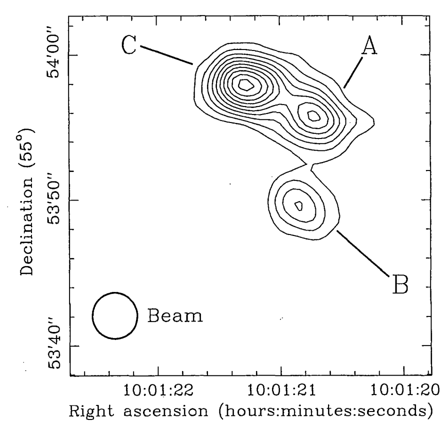

Fig. 1. Radio continuum contour map of the lensed quasar 0957+561, at a wavelength of 3.1 mm. Source C is the radio continuum jet associated with image A of the quasar. The lensing galaxy is located ~1″ north of image B (*11*). Contour levels are in steps of 0.5 mJy per beam, ranging from 0.5 to 5.0 mJy per beam. The absolute position of sources A and B coincides with that of the VLA (*13*) measurements, within measurement uncertainties. The synthesized beam of 3.2″ by 3.1″ is shown in the lower left corner.

[1]Observatorio Astronómico Nacional (IGN), Apartado 1143, E-28800 Alcalá de Henares, Spain. [2]Institut de Radio Astronomie Millimétrique, F-38460 Saint Martin d'Hères, France. [3]Instituto de Física de Cantabria (CSIC-UC), Facultad de Ciencias, E-39005 Santander, Spain.

*To whom correspondence should be addressed. E-mail: planesas@oan.es

Melting Dynamics Beneath the Tonga-Kermadec Island Arc Inferred from ²³¹ Pa- ²³⁵ U Systematics
Bernard Bourdon; Simon Turner; Claude Allegre
Science, New Series, Vol. 286, No. 5449. (Dec. 24, 1999), pp. 2491-2493.
Stable URL:
http://links.jstor.org/sici?sici=0036-8075%2819991224%293%3A286%3A5449%3C2491%3AMDBTTI%3E2.0.CO%3B2-5

This article references the following linked citations:

References and Notes

[1] **U-Th Isotopes in Arc Magmas: Implications for Element Transfer from the Subducted Crust**
C. J. Hawkesworth; S. P. Turner; F. McDermott; D. W. Peate; P. van Calsteren
Science, New Series, Vol. 276, No. 5312. (Apr. 25, 1997), pp. 551-555.
Stable URL:
http://links.jstor.org/sici?sici=0036-8075%2819970425%293%3A276%3A5312%3C551%3AUIIAMI%3E2.0.CO%3B2-M